# The Transient Complex of Cytochrome c and Cytochrome c Peroxidase: Insights into the Encounter Complex from Multifrequency EPR and NMR Spectroscopy**

Martin van Son,[a] Jesika T. Schilder,[b] Antonella Di Savino,[b] Anneloes Blok,[b] Marcellus Ubbink,[b] and Martina Huber*[a]

We present a novel approach to study transient protein-protein complexes with standard, 9 GHz, and high-field, 95 GHz, electron paramagnetic resonance (EPR) and paramagnetic NMR at ambient temperatures and in solution. We apply it to the complex of yeast mitochondrial iso-1-cytochrome *c* (Cc) with cytochrome *c* peroxidase (CcP) with the spin label [1-oxyl-2,2,5,5-tetramethyl-Δ3-pyrroline-3-methyl)-methanethiosulfonate] attached at position 81 of Cc (SL–Cc). A dissociation constant $K_D$ of $20 \pm 4 \times 10^{-6}$ M (EPR and NMR) and an equal amount of stereo-specific and encounter complex (NMR) are found. The EPR spectrum of the fully bound complex reveals that the encounter complex has a significant population (60%) that shares important features, such as the Cc-interaction surface, with the stereo-specific complex.

## 1. Introduction

Transient protein-protein complexes have a critical role in the transmission and integration of biochemical signals in the cell. They are often involved in electron transfer (ET) and evolved to provide fast turnover in the crowded cellular environment.[2] For this reason, transient complexes, ET complexes in particular, typically exhibit weak binding with a dissociation constant ($K_D$) in the μM-mM range.[3] The formation of transient complexes has been demonstrated to involve an encounter complex (Figure 1B), an ensemble of orientations in fast exchange, in which the proteins sample their respective surfaces in search of the binding site. This highly dynamic state[4] is called "productive" if it leads to the stereo-specific complex (Figure 1C)[1,5,6] or "futile"[4,7–10] otherwise.

To briefly introduce the terminology, we refer to the stereo-specific complex as the complex with the structure as observed in the crystal structure of the complex (Figure 1). The encounter complex is the ensemble of other orientations that the two proteins assume. So the distinction can be strong, in cases where the stereo-specific complex is there a large fraction of the time and the encounter complex represents only a small fraction (e.g. for the cytochrome P450cam:putidaredoxin complex).[11] It can also be vague in the cases of cytochrome *f*: plastocyanin complexes[12–15] or absent, for example in the complex of myoglobin and cytochrome $b_5$[16] or cytochrome *c* and adrenodoxin[17,18] or cytochrome *c* and plastocyanin.[19] To illustrate, in the complex investigated in the present study, a significant fraction (70% for wild type) still seems to be in a single, stereo-specific complex and the remainder in the encounter complex (see below).

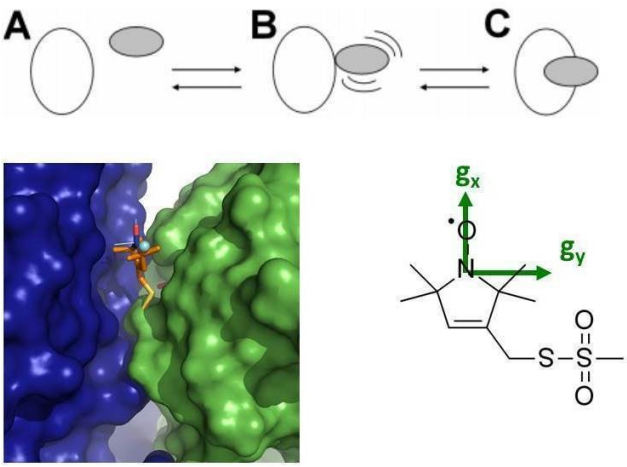


**Figure 1.** Top: Scheme of protein interaction in a transient protein complex. Free partner proteins (A), encounter complex (B), in which the proteins are able to sample their respective surfaces. The encounter complex is in equilibrium with a tightly bound stereo-specific complex (C). The figure concerns an edited version of that in reference 1. Bottom left: Binding site with spin label: blue: CcP surface, green: Cc-surface with spin label attached, the vector connecting the nitrogen and the cyan sphere indicates the direction of the $g_y$ axis, right: MTLS spin label with approximate g-tensor axis directions.

Previous experiments suggest that the initial stage of the formation of the encounter complex is governed mostly by

[a] M. van Son, Dr. M. Huber
Leiden Institute of Physics, Huygens-Kamerlingh Onnes Laboratory, Leiden University, Niels Bohrweg 2, 2333 CA Leiden (The Netherlands)
E-mail: huber@physics.leidenuniv.nl
[b] J. T. Schilder, A. Di Savino, A. Blok, Prof. M. Ubbink
Leiden Institute of Chemistry, Leiden University, Gorlaeus Laboratories, Einsteinweg 55, 2333 CC Leiden (The Netherlands)

[**] EPR: Electron Paramagnetic Resonance

Supporting information for this article is available on the WWW under https://doi.org/10.1002/cphc.201901160

long-range electrostatic interactions,[20,21] but hydrophobic interactions can in some cases be relevant.[8,15,22] Guiding the proteins through these interactions, the encounter complex can enhance the formation of the stereo-specific complex by reducing the search area. Paramagnetic NMR gave an important contribution in the characterization of the encounter states[2,23–24] but has limitations with respect to extracting structural information on the encounter complex. Encounter states are invisible to standard techniques for structural characterization of biomolecules (X-ray crystallography, electron microscopy, mass spectrometry, traditional NMR), so new methods are sought to investigate their properties. Here, we present an EPR approach to study such transient complexes, which pose challenges not encountered for high-affinity complexes, such as barnase with barstar,[25] investigated by EPR previously. A 9 GHz EPR study of the complex of cytochrome $bc_1$ with cytochrome *c* was described.[26,27]

We investigate the complex of yeast mitochondrial iso-1-cytochrome *c* (Cc) with cytochrome *c* peroxidase (CcP), which, in yeast, has its main function in the removal of hydrogen peroxide. Recently, CcP was reported also to work as a mitochondrial $H_2O_2$ sensor[28,29] and to be involved in haem storage.[30] The encounter state between Cc and CcP can be described using exclusively electrostatic interactions, and paramagnetic NMR experiments revealed that Cc samples just 15% of the CcP surface to find the binding site.[31] Furthermore, PRE experiments showed that the encounter complex between Cc and CcP is populated for 30% of the time, while the stereo-specific, crystallographic complex,[32] has 70% occupancy.[1,31] It was also found that the encounter state can heavily influence the stability of the protein complex. In fact, point mutations on the Cc binding surface for CcP were able to change the equilibrium between stereo-specific and encounter state, reducing the population of latter to 10%, or making it the predominant state with the 80% occupancy. As a consequence, the binding constant ($K_B$) of the complex was affected. The $K_B$ for the mutants described in reference[33] varied from a 9-fold enhancement to a 30-fold reduction compared to the wild type.[33] These studies indicate that the balance between encounter complex and stereo-specific complex is a delicate one. Although the Cc–CcP complex is one of the best studied ET complexes, the model of the ET activity is still matter of debate. Besides the model describing the ET transfer through the stereo-specific complex,[34,35] ET could occur through another, not overlapping, low-affinity site at low ionic strength, being abolished at ionic strength values larger than 100 mM. Binding of Cc at this site would allow a faster ET than the high-affinity binding site.[36,37] Paramagnetic NMR experiments have enabled the characterisation of the low-affinity interaction site, revealing that the weak complex is composed of different species: a dominant population with a distance of 22 Å between the haems, which is therefore probably inactive in ET, and an ensemble of species that could be functional because the haems are less than 16 Å apart.[38,39]

With a dissociation rate constant of about 1000 $s^{-1}$,[40,41] all processes of formation of the encounter complex, transition to the stereo-specific complex and dissociation are fast on the NMR timescale. Thus, only averages of chemical shift perturbations and relaxation rates are obtained, limiting the possibilities to characterize the encounter state without additional modelling. The timescale of electron paramagnetic resonance (EPR) is five orders of magnitude faster, in the nano-second regime, and therefore can be expected to give complementary information.

Here, we investigate whether EPR can help to characterize the encounter complex, making use of the sensitivity of continuous-wave (cw) EPR to the nanosecond motion of a nitroxide spin label. The spin label was attached covalently to the smaller protein in the complex, the Cc, similar to the approach used by Sarewicz *et al.*[26,27] By monitoring the complex with a spin label attached to the smaller protein, the changes in rotation-correlation time ($\tau_r$) upon complex formation are maximized. We attached the spin label to an engineered cysteine, mutant A81C of Cc (Cc–SL). In contrast to [63], we probe complex formation at room temperature, where the proteins are in their physiological state.

We present a systematic approach to analyse the EPR spectra: We determine the dissociation constant of the complex, and the EPR spectra of the complex in the fully-bound state. This is challenging because the EPR spectra of the spin label cannot be described by a simple lineshape function (Gaussian or Lorentzian), and the spectra of free Cc–SL and Cc–SL bound to CcP have significant overlap. Particularly, it is not trivial to extract the spectrum of the fully-bound state, because the EPR spectra of samples containing both partners always contain a fraction in which the spin-labelled partner is not in the complex (free Cc–SL), even at a large excess of the complex partner (CcP). To overcome this problem, we make use of principal component analysis (PCA)[42] and linear prediction methods.

We find that the spin label in the A81C-variant of Cc becomes immobilized upon complex formation. The interaction surface of Cc with CcP encompasses residue 81. According to EPR, the encounter complex has two fractions, with a dominant one (60%) in which Cc exposes the same surface to CcP as in the stereo-specific complex. This suggests that the majority fraction of the encounter complex bears similarity to the stereo-specific complex, a finding that is a first step to derive structural detail on the encounter complex that was so far elusive. In the second fraction of the encounter complex, the spin label has more freedom to move, suggesting a more loosely bound complex and possibly a different interaction surface of Cc with CcP. The lifetime of the two conformations of the encounter complex exceeds 3 ns, showing that also more detail on the dynamics of the encounter complex can be obtained by the combined NMR and EPR approach.

## 2. Materials and Methods

### 2.1. Production and Purification of CcP C128 A

A pET28aCcP plasmid containing the gene encoding *S. cerevisiae* CcP1 with mutation C128 A was used to produce unlabelled or [$^{15}N$–$^{2}H$] labelled CcP. Production and purification have been described in [43]. The resulting protein was ~80%

deuterated, as estimated from 1D $^1$H NMR. The concentration of CcP was determined using UV-Vis spectroscopy at $\varepsilon_{408nm} = 98\ mM^{-1}cm^{-1}$.[40] The yield was approximately 130 mg/L in minimal media.

### 2.2. Expression and Purification of Cc A81C

A pUC19 based plasmid containing the genes encoding *S. cerevisiae* iso-1-cytochrome *c* as well as haem lyase was used to express and purify Cc as described previously.[44,45] The wild type (WT) protein and mutant A81C[46] were used. The concentration of Cc was determined using UV-Vis spectroscopy and $\varepsilon_{410nm} = 106.1\ mM^{-1}cm^{-1}$.[45] The yield was approximately 20 mg/L in rich media.

### 2.3. Cc A81C Spin Labelling

For EPR experiments, Cc A81C (1 mL of 822 μM) was reduced with 5 mM DTT at 4 °C for 60 minutes. DTT was removed with a 5 mL desalting column (GE Healthcare) equilibrated in 100 mM $NaP_i$, pH 7.2, 100 mM NaCl (argon bubbled to remove oxygen). Immediately after elution, Cc A81C was added to a solution of 20 mL 100 mM $NaP_i$ pH 7.2, 100 mM NaCl, 2.2 mM [1-oxyl-2,2,5,5-tetramethyl-δ-3-pyrroline-3-methyl)-methanethiosulfonate] (Toronto Research Chemicals, North York, ON, Canada), MTSL. This solution was kept at 4 °C for 1 hour while bubbling with argon. The total volume of 23 mL was concentrated to 0.85 mL and kept overnight at 4 °C. Free MTSL was removed by a Superdex 75 gel filtration column (GE Healthcare) equilibrated in 100 mM $NaP_i$ pH 7.2, 100 mM NaCl. The absorption was monitored at 280, 410, and 550 nm and fractions of 1 mL were collected. Fractions with an $A_{550}/A_{280}$ ratio larger than 0.80 were combined and concentrated to 0.7 mL. To the protein solution 5 mM $K_3[Fe_3(CN)_6]$ was added. After 60 minutes, the oxidizing agent was removed by a PD10 column. The protein solution was concentrated to 0.6 mL. EPR experiments showed that approximately 93 % of the Cc carried a paramagnetic label. The protein solution was flash-frozen in liquid $N_2$ and stored at −80 °C. For NMR experiments, the procedure was similar. Details are given in [43]. MTS [1-acetoxy-2,2,5,5-tetramethyl-δ-3-pyrroline-3-methyl)-methanethiosulfonate] was used in this case to generate the diamagnetic control sample for NMR titrations.

### 2.4. EPR-Sample Preparation

All EPR samples were prepared in 20 mM $NaP_i$, 100 mM NaCl, pH 6.0, with protein concentrations based on UV-Vis absorption. For 9 GHz measurements, the samples containing 100 μM Cc and varying concentrations of CcP were transferred into 50 μL micropipettes (BLAUBRAND® intraMARK) with an inner/outer diameter (id/od) of 0.80 mm/1.50 mm. For 95 GHz measurements at room temperature the concentration of spin-labelled Cc was 0.4 mM and samples were placed in suprasil quartz capillaries (Wilmad-Labglass, Buena, NJ, USA) with an id/od of 0.1 mm/0.5 mm. This capillary was put into a suprasil quartz capillary (VitroCom, Mountain Lakes, NJ, USA) with an id/od of 0.60 mm/0.84 mm. At both ends the capillaries were sealed with X-Sealant®. For 95 GHz measurements at 80 K the concentration of spin-labelled Cc (Cc–SL) was 0.4 mM and samples were placed in suprasil quartz capillaries (VitroCom, Mountain Lakes, NJ, USA) with an id/od of 0.60 mm/0.84 mm. Both ends were sealed with an epoxy polymer.

### 2.5. 9 GHz EPR Measurements

Measurements at 9 GHz were performed using an ELEXSYS E 680 spectrometer (Bruker BioSpin GmbH, Rheinstetten, GE) equipped with a rectangular cavity. Spectra were recorded at 0.63 mW microwave power with a modulation amplitude/frequency of 0.2 mT/100 kHz. A 15 mT field sweep of 2048 points was used with a time constant of 10 ms. The total measurement time for a spectrum varied between 35 and 80 minutes. A gentle stream of $N_2$ was blown through the cavity. A chrome/alumel thermocouple was installed close to the sample to monitor the temperature with a readability of 0.1 K. The temperature during the 9 GHz measurements was 292.6 ± 0.1 K.

### 2.6. EPR Measurements at 95 GHz

For 95 GHz measurements at room temperature and 80 K a locally developed probe head was used combined with a Bruker Elexsys 680 (Bruker BioSpin GmbH, Rheinstetten, Germany) spectrometer. Measurements were performed with a modulation amplitude of 0.3 mT (95 GHz, RT), and 0.2 mT (95 GHz, 80 K) and a modulation frequency of 10 kHz (95 GHz, RT and 80 K). The time constant was 82 ms (95 GHz, RT), and 41 ms (95 GHz, 80 K). Spectra were recorded with a 30 mT field sweep of 4096 points (95 GHz, RT), and a 40 mT field sweep of 4096 points (95 GHz, 80 K). The total measurement time for a recorded spectrum was 120 minutes (95 GHz, RT), and 10 minutes (95 GHz, 80 K).

### 2.7. NMR Spectroscopy, Titration Experiments

To obtain binding constants, 1.7–2.5 mM stocks of WT or MTS-A81C Cc were titrated into 400 μM $^{15}N$–$^2H$–CcP (~80 % deuterated) in 20 mM NaPi, 100 mM NaCl, 6 % $D_2O$, pH 6.0. 2D BEST-TROSY-HSQC experiments[47] were recorded on a Bruker AVIII HD spectrometer equipped with a $^1H(^{13}C/^{15}N)$ TCI-cryoprobe, operating at a proton Larmor frequency of 850 MHz at 293 K with 1024 and 100 complex points in the $^1H$ and $^{15}N$ dimensions, respectively. Spectra were recorded at intervals of 0.2:1 Cc:CcP until a final ratio of Cc:CcP of 2.0:1 was reached. All data were processed using Topspin 3.2 (Bruker, Karlsruhe, Germany) and analysis was done using CCPN analysis 2.1.5.

The average CSP ($\Delta\delta_{avg}$) were derived as described previously.[48] The chemical shift titration curves were analyzed with a two-parameter, non-linear least squares fit using a one-

site binding model as described previously.[49] The fitting was done using OriginPro 8.5 (OriginLab, Northampton, USA).

### 2.8. Equations to Calculate $K_D$ from the Fraction of Bound Complex *c*

Complex formation and dissociation are described by the equilibrium reaction

$$LP \rightleftarrows L + P \tag{1}$$

where $L$ and $P$ are the complex partners. The dissociation constant $K_D$ is defined as

$$K_D = \frac{[L][P]}{[LP]}, \tag{2}$$

where $[L]$ is the concentration of $L$ Equation 2 is rewritten using the total concentrations $[L]_0$ and $[P]_0$:

$$K_D = \frac{(1-c)[L]_0([P]_0 - c[L]_0)}{c[L]_0}, \tag{3}$$

where $c$ is the fraction of $L$ that is bound to $P$. In the case that $c$ is unknown, equation 3 is more conveniently written as

$$c = 0.5[L]_0^{-1}\left\{\begin{array}{l} K_D + [L]_0 + [P]_0 - \\ \sqrt{K_D^2 + 2K_D([L]_0 + [P]_0) + ([L]_0 - [P]_0)^2} \end{array}\right\} \tag{4}$$

### 2.9. Linear Decomposition

The experimental spectrum $\vec{E}$ is composed of the free spectrum $\vec{F}$ and the bound spectrum $\vec{B}$

$$\vec{E} = f\vec{F} + b\vec{B} \tag{5}$$

where $f$ is the fraction of Cc–SL that is free and $b$ is the fraction bound, i.e., Cc–SL in complex with CcP. Thus, we can use equation (5) to obtain the bound spectrum from the experimental spectrum. For this procedure, the EPR spectra are required to be normalized and superimposed such that the central lines overlap.

### 2.10. Simulation of EPR Spectra

The cw-EPR spectra were simulated with EasySpin,[50] a software package for MATLAB (The Mathworks, Natick, MA, USA). We manually adjusted the parameters to maximize the similarity between the simulated and the experimental spectrum.

The algorithm *Pepper* was used for the simulation of the 95 GHz spectrum of free Cc–SL in frozen solution, recorded at 80 K. From this simulation the following spin parameters were obtained: $A_N = [A_{xx}\ A_{yy}\ A_{zz}] = [16.0\ 15.0\ 104.1]$ MHz, $g = [g_{xx}\ g_{yy}\ g_{zz}] = [2.0088\ 2.0066\ 2.0028]$. These values were then used for all other simulations.

The algorithm *Garlic* was used for the solution spectra recorded at room temperature. This algorithm allows for the adjustment of the rotation-correlation time, $\tau_r = [\tau_{xx}\ \tau_{yy}\ \tau_{zz}]$. We found that the solution spectra are best simulated with two components – one component that represents a fast mobility, the other a slow mobility. We used two restrictions in our approach to simulate the spectra of free Cc–SL: i) the $\tau_r$ and the ratio of two components were taken equal for the spectra in 9 GHz and 95 GHz; ii) the fast and slow component were simulated with an anisotropic and an isotropic rotation component, respectively. The same approach was used in the simulation of the 9 GHz and 95 GHz spectra of bound Cc–SL.

### 2.11. The Protein Rotation-Correlation Time

For a globular protein with radius $r$, the rotation-correlation time is calculated using the Stokes-Einstein relation

$$\tau_r = \frac{4\pi r^3 \eta}{3k_B T} \tag{6}$$

where $\eta$ is the viscosity of water (1.00 mP·s), $k_B$ the Boltzmann constant, and $T$ is the temperature, in this work: $293 \pm 1$ K. The radius of Cc and that of the complex was measured from the coordinates of the crystal structure of the Cc:CcP complex (PDB entry 2PCC[32]). A hydration radius of 2.4 Å was taken into account.

Calculation with HYDRO NMR[51] based on PDB entry 2PCC[32] was used as an alternative route to calculate the isotropic $\tau_r$ of Cc and the complex.

## 3. Results

### 3.1. NMR Chemical Shift Perturbation Titration

To determine whether attachment of the tag to the cysteine at position 81 of Cc affects complex formation, WT and A81C-MTS Cc were titrated into $^{15}N$–$^{2}H$–CcP and chemical shift perturbations (CSP) were monitored. During the titrations many resonances shifted with increasing concentration of Cc, indicating a binding process in the fast-exchange regime.

The $K_D$ determined using a 1:1 binding model for WT Cc is $5 \pm 2 \times 10^{-6}$ M, in accord with previously reported values (Figure 2).[40,52] For MTS-A81C, the binding was found to be slightly weaker with $K_D = 20 \pm 4 \times 10^{-6}$ M. These $K_D$ values were then used to extrapolate average amide shifts, $\Delta\delta_{avg}$, for 100% bound CcP. For the WT complex, the overall CSP pattern was similar to that described previously.[53] The CSPs for WT and MTS-A81C show that the binding site is conserved but some differences outside the error margins ($\pm 0.016$ ppm) are observed, listed in Table S1. From the plot of the differences in CSPs for A81C-MST Cc and WT Cc (Figure S2), it is clear that

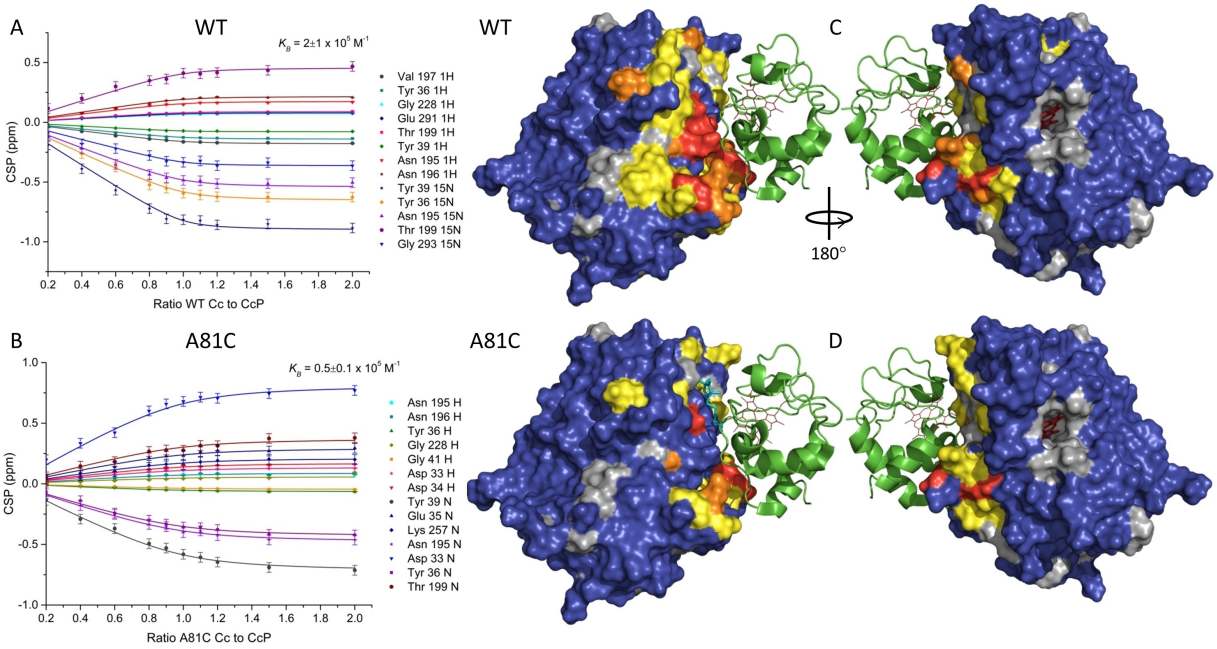


**Figure 2.** Chemical shift perturbations for selected CcP residues in the $^1$H or $^{15}$N dimension during titration with WT Cc **(A, C)** or MTS-A81C Cc **(B, D)**. **A, B)** Binding curves were fitted globally to a 1:1 binding model and the solid lines show the best fit when using a shared $K_B$ (=1/$K_D$) value. **B, D)** Chemical shift perturbation map for $^{15}$N–$^2$H–CcP C128A bound to WT **(B)** or MTS-A81C Cc **(D)** colour coded on a surface model of CcP (haem group in red sticks) in the stereospecific complex (PDB-entry 2GB8).[1] Cc is shown in green ribbons with the haem group in red lines and a model for the MTSL is shown in teal sticks. CSP were extrapolated to 100% bound CcP. Residues with $\Delta\delta_{avg} \geq 0.06$ ppm are red, 0.04–0.06 ppm are orange, 0.02–0.04 ppm are yellow, 0–0.02 ppm are blue and with no data are grey. These experiments were done in 20 mM NaPi, 100 mM NaCl (pH 6) at 293 K. The data for WT were reported before in [43] and are shown for comparison.

many of the shifts are somewhat smaller for the former. This is also reflected in the CSP map on the surface of CcP (Figure 2). The slightly weaker binding and the smaller CSPs (after extrapolation to 100% bound CcP) can indicate that the equilibrium between encounter state and stereo-specific state has shifted somewhat to the encounter state. It has been shown that lowering the binding constant of this complex increases the fraction in the encounter state. In particular, the mutation R13 K on Cc, which has a very similar binding constant to MTS-A81C ($K_D = 18 \pm 1 \times 10^{-6}$ M), shifted the equilibrium to 50% encounter/50% stereo-specific complex;[33] this is likely also the case here.

### 3.2. Results of EPR Measurements on the Complex

Figure 3 shows a series of 9 GHz EPR spectra of spin-labelled cytochrome *c* (Cc–SL) measured in the presence of increasing concentrations of cytochrome *c* peroxidase (CcP). The spectrum in Figure 3a is that of free Cc–SL and shows three lines. With CcP added, additional features appear (indicated by arrows in Figure 3b to g). With increasing CcP concentration, the intensity of these features increases and the signal intensity of free Cc–SL decreases. A control experiment at high salt concentration of Cc–SL with an excess of CcP (1:3 ratio) is shown in yellow in Figure 3a. This spectrum is identical to that of free Cc–SL, emphasizing that the spectral changes observed in the spectra in Figure 3b–g are due to complex formation, as high ionic strength inhibits complex formation. Similarly, the Cc–SL EPR spectra are hardly perturbed by bovine serum albumin, a protein that does not form a complex with Cc (see SI), showing

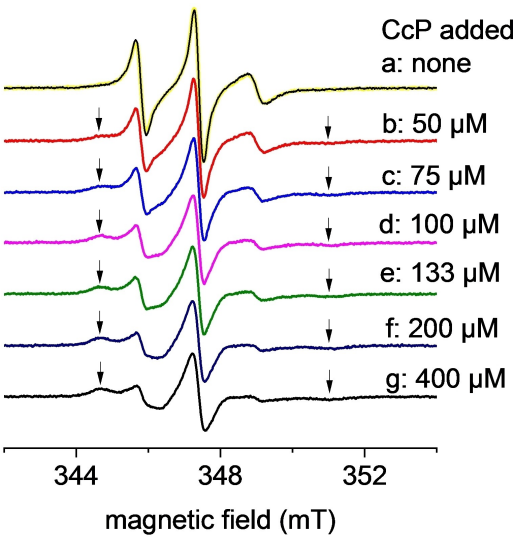


**Figure 3.** The 9 GHz room-temperature EPR spectra of spin-labelled cytochrome *c* (Cc–SL) with different concentrations of CcP added. (a) 100 µM Cc–SL without CcP, (b) 100 µM with 50 µM CcP, (c) with 75 µM CcP, (d) with 100 µM CcP, (e) with 133 µM CcP, (f) with 200 µM CcP, and (g) with 400 µM CcP. The arrows indicate lines in spectra (b) to (g) that are not present in spectrum (a). Spectrum (a) is overlaid with the spectrum of 135 µM Cc–SL, 388 µM CcP with 556 mM NaCl (in yellow).

again that the changes observed in Figures 3 and 4 are due to complex formation between Cc and CcP.

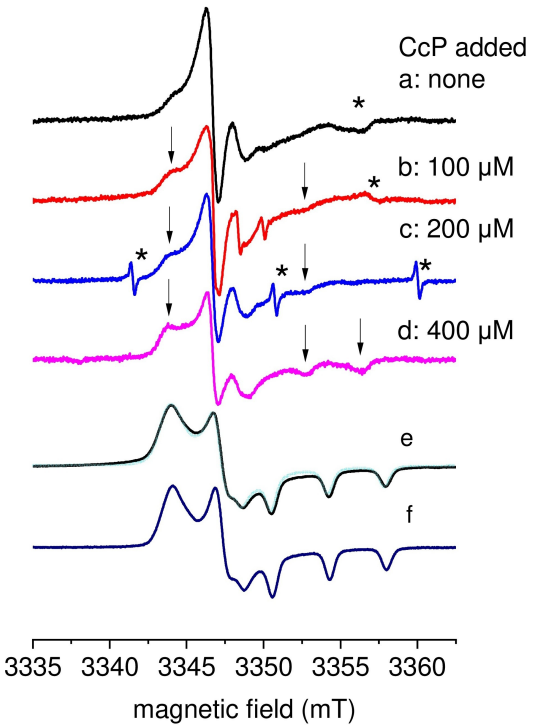


**Figure 4.** The 95 GHz EPR spectra of Cc–SL with different concentrations of CcP at room temperature (RT) and at 80 K. 400 μM Cc–SL (a) without CcP (RT), (b) with 100 μM CcP (RT), (c) with 200 μM CcP (RT), (d) 414 μM Cc–SL with 400 μM CcP (RT), (e) 482 μM Cc–SL without CcP (80 K), and (f) 371 μM Cc–SL with 373 μM CcP (80 K). In the room-temperature spectra, the arrows indicate lines that are more pronounced than in the spectrum shown in (a). The asterisk in (a) and (b) indicates a background signal. The asterisks in (c) indicate sharp lines that likely originate from a manganese impurity. The spectrum of free Cc–SL recorded at 80 K, shown in (e), was used for simulation (in cyan) to obtain the $\boldsymbol{G}$ and $A_N$ tensor given in Materials and methods.

Figure 4 shows the 95 GHz EPR spectra of Cc–SL measured with different concentrations of CcP. With CcP added, features are visible (indicated by arrows in Figure 4b to d) that correspond to a signal with broader lines than the free Cc–SL (Figure 4a), particularly in the high-field region.

The frozen-solution spectra of Cc–SL (Figure 4e) and Cc–SL:CcP 1:1 (Figure 4f) have singularities at identical field positions revealing that the $\boldsymbol{G}$ and $\boldsymbol{A}_N$ tensor parameters of free Cc–SL and Cc–SL bound to CcP do not differ significantly in the frozen state. Therefore, $\boldsymbol{G}$ and $\boldsymbol{A}_N$ parameters for the simulation of the solution spectra were derived from the simulation of the spectrum in Figure 4e.

Principal Component Analysis (PCA), performed as described in the SI, on the series of 9 GHz EPR spectra shown in Figure 3, reveals that the EPR spectra contain two components only. The spectrum of the fully bound Cc–SL, extracted by PCA, is shown in Figure 5. The fraction of bound Cc–SL derived from the PCA analysis was used to determine the dissociation constant of the complex $K_D$ The $K_D$ that best fits these data (equation 4) is $K_D = 17 \pm 3$ μM. For comparison, $K_D$ was also determined from the fraction of bound Cc–SL derived from linear decomposition, which resulted in a $K_D$ that is identical to that derived from PCA, as described in the SI.

The 95 GHz EPR spectra showed four principal components in PCA, rather than the two components expected from the results of the 9 GHz EPR spectra. We attribute the additional components to spurious signals and baseline instabilities, which are more pronounced in the 95 GHz than in the 9 GHz EPR spectra, and therefore abandoned PCA on the 95 GHz EPR spectra. For the 95 GHz EPR spectra, analysis by linear decomposition works better. To extract the fully bound spectrum, a fraction of the spectrum of free Cc–SL (Figure 4a) was subtracted from the spectrum in Figure 4d. The amount of free spectrum was varied in the range of 10% to 50% and the value of 20% was selected by visual inspection, resulting in the spectrum shown in Figure 5d.

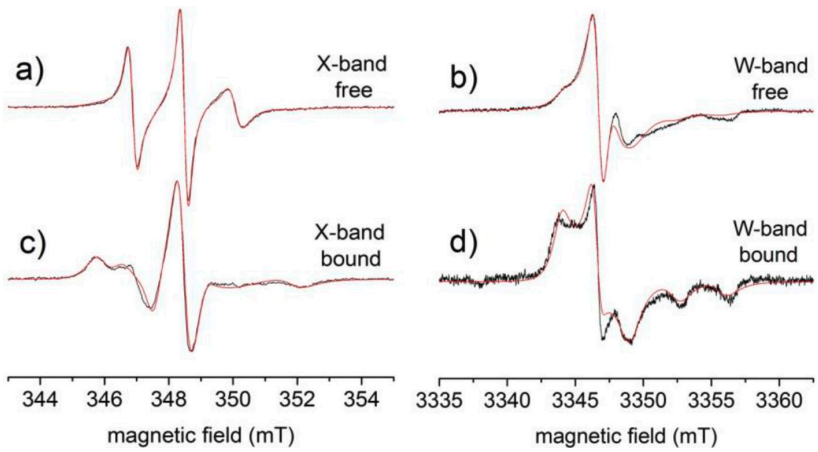


**Figure 5.** The EPR spectra of Cc–SL in the free form (a) and b)) and of Cc–SL fully bound to CcP (c) and d)) at 9 GHz and 95 GHz. The experimental and simulated data are shown in black and red, respectively. The experimental data in a) and b) are spectra directly obtained from measurement. The experimental data in c) was obtained via PCA (see SI) applied to the spectra shown in Figure 3. The experimental data in d) was obtained via linear decomposition (see Materials and methods) of the spectra shown in Figures 4a and d. The simulations were obtained with the parameters listed in Table 1. Note: for the spectra in a) and c) an up-field shift of 1.1 mT was applied compared to the spectra in Figure 3.

Rotation-correlation times of the spin label were determined by simulations of the spectra of free Cc–SL and of Cc–SL fully bound to CcP (Cc–SL:CcP, Figure 5). The parameter set given in Table 1 fits best to the 9 GHz and the 95 GHz spectra simultaneously. To satisfactorily simulate the 9 GHz and the 95 GHz spectra, two components were used, one of which had a rhombic rotation tensor. Models including an ordering potential[54] were not tried. In free Cc–SL, a majority fraction (60%) of the spin label rotates with a $\tau_r$ that is anisotropic and overall smaller than the $\tau_r$ of the protein (Table 1). The second fraction is isotropic and has a $\tau_r$ close to that of the protein.

In the fully-bound state, the rotation is slower than for free Cc–SL. The larger fraction (80%) has an isotropic rotation with a $\tau_r$ of 8 ns, and the smaller fraction has an anisotropic rotation, with an average $\tau_r$ that is about twice as long as that of the fast fraction in the free Cc–SL. The anisotropic rotation has the smallest component along the y-axis of the nitroxide in the simulations of the spectra of free Cc–SL and of Cc–SL fully bound to CcP. Simulation parameters may not be unique, and, in particular, several solutions for the anisotropy of the rotation were found, which agree with the data. Figure 6 shows the same experimental spectra as in Figures 5c and d and simulations of the spectra, which were obtained with an isotropic $\tau_r$ of 8 ns, i.e. omitting the minor component from the simulations. The agreement between experiment and simulation in Figures 6a and b is less than in Figures 5c and d, a discrepancy that is particularly pronounced for the 95 GHz EPR spectra, which emphasizes the need for the minor component to represent the spectra well.

## 4. Discussion

We investigated the complex of Cc with CcP by liquid solution, 9 and 95 GHz EPR on a spin labelled variant of Cc, Cc–SL. We determined the properties of the complex of the same construct with NMR, from which we derive the relative amounts of encounter and stereo-specific complex. Combining both approaches, we obtain information on the dynamics of the complex and the interaction surface of Cc with CcP in the stereo-specific and the encounter complex.

In the complex of wild type Cc with spin labels linked to the surface of CcP, 30% of the complex is in the encounter state and 70% in the stereo-specific state.[1,31] Attachment of the spin label to Cc residue 81 reduces the affinity for binding to CcP four-fold ($K_D = 20 \pm 4$ μM) and the CSP map on the surface of CcP suggests that the encounter state is more populated than with wild type Cc, estimated to be around 50%. Mutations of Cc residues in the interface of the stereo-specific complex similarly showed a correlation between the fraction of encounter complex with the binding affinity.[33]

Combining 9 GHz and 95 GHz EPR at room temperature, the changes in motion of the spin label attached to Cc (Cc–SL) that occur when Cc–SL is in the presence of the complex-binding partner (CcP) are detected, Figures 3 and 4. Control experiments show that these changes are due to complex formation.

To map the change in spin-label motion in the free and fully bound state of Cc–SL, spectral analysis is performed. In particular, the spectrum of Cc–SL in complex with CcP needs attention, because mixtures of Cc–SL and CcP always contain a fraction of free Cc–SL, even at a large excess of CcP. A

**Table 1.** The parameters used for the simulation of cw-EPR spectra of spin-labelled cytochrome *c* (Cc–SL) alone (free) and in complex with cytochrome *c* peroxidase (CcP) (bound).

| | Fast component[a] | | | | | Slow component[a] | | Protein/complex | |
|---|---|---|---|---|---|---|---|---|---|
| State of Cc–SL | $\tau_{xx}$ [ns] | $\tau_{yy}$ [ns] | $\tau_{zz}$ [ns] | Isotropic $\tau_r$[ns] | Fraction | Isotropic $\tau_r$[ns] | Fraction | Isotropic $\tau_r$[ns] | |
| free | 2.0 | 0.7 | 3.0 | 1.3 | 60% | 5.0 | 40% | 5.6[b] | 7.3[c] |
| bound | 8.0 | 1.5 | 8.0 | 3.3 | 20% | 8.0 | 80% | 18.5[b] | 29[c] |

[a] The spectral lines were described with a Gaussian (g) and/or Lorentzian (l) lineshape. The linewidths used were: 9 GHz free: 0.03 mT (g), 0.04 mT (l)/95 GHz free: 0.3 mT (l)/9 GHz bound: 0.07 mT (g)/95 GHz bound: 0.1 mT (l). [b] The values were calculated with equation (6). [c] The values were calculated with HYDRO NMR[51] (see Materials and methods).

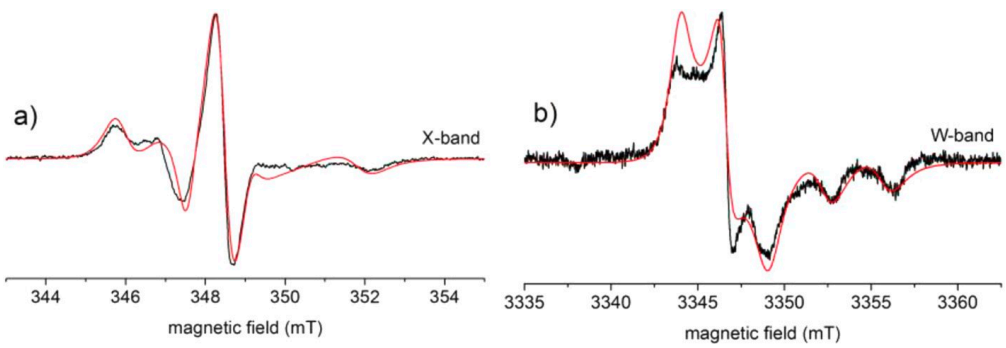


**Figure 6.** Simulations of the EPR spectra of Cc–SL fully bound to CcP, showing the effect of the fast component on the spectra. Simulations (red) of 9 GHz (a) and 95 GHz (b) spectrum without the fast component, i.e. using only an isotropic rotation-correlation time of 8 ns. The experimental spectra are identical to the spectra in Figures 5c and d.

contribution of free Cc–SL in the order of 5% remains, and, since the spectrum of free Cc–SL has narrower lines than that of Cc–SL in complex with CcP, the free Cc–SL contribution disturbs the lineshape. We used PCA and linear decomposition to determine the EPR spectrum of bound Cc–SL and the fraction by which this spectrum contributes to the experimental spectra of mixtures of Cc–SL with different ratios of CcP. The fraction of bound Cc–SL serves to determine the $K_D$-value (see Results). The $K_D$ thus obtained ($17 \pm 3$ μM) agrees with the results of the NMR experiments: $K_D = 20 \pm 4$ μM, showing that EPR and NMR monitor the same state of the complex.

Spin-label dynamics of free Cc–SL and fully bound Cc–SL differ considerably. The free Cc–SL has two components that differ in the mobility of the spin label. Two mobility components are often observed in spin label EPR, see for example,[55–62] and are interpreted as conformations in which the spin label experiences different constraints from the protein. In the case of the free Cc–SL, the majority fraction has a high mobility and the rotation-correlation time of the spin label is smaller than that of the protein, showing that local mobility, i.e., rotation about the single bonds linking the spin label to the protein backbone (Figure 1), is dominant in that fraction. The local motion is much reduced in the second fraction, in which the nitroxide is locked to the protein, for example through interaction with residues at the protein surface. The spin label is either completely immobilized at the protein surface, or, if it has residual motion, the correlation time of this motion must be larger than 5.6 ns, the $\tau_r$ of the protein.

When Cc–SL is in complex with CcP, the local mobility of the spin label is reduced, leading to larger $\tau_r$ values and a smaller fraction of the mobile form (20% compared to 60% in the free form). The parameters observed in the bound state are incompatible with those of Cc–SL in the free state, showing clearly that spin-label dynamics is determined by the interaction with the complex partner, not, for example, the protein surface of the Cc itself.

To demonstrate the validity of the interpretation of two fractions, in Figure 6 we compare the fully bound spectrum with simulations in which the mobile fraction is omitted. Notably, the simulation of the 9 GHz spectrum is still acceptable, but the 95 GHz spectrum is not compatible with that interpretation. This demonstrates that by high-field EPR previously inaccessible details of complex formation can be determined. The fast fraction is explained by local mobility, implying a conformation in which the pyrroline ring of the spin label has some freedom to move. By virtue of the higher resolution of 95 GHz EPR, also details of this motion are determined: the motion is dominated by a faster rotation about the spin label $g_{yy}$ axis (see Figure 1), suggesting that the spin label is more free to rotate about this axis. Rotation about both the $g_{xx}$ and the $g_{zz}$ axes is significantly slower.

The second component observed in the EPR spectra of Cc–SL:CcP, the slow, and majority fraction, is explained by pinning, or inhibition of the pyrroline-ring motion in the interface between Cc and CcP, which shows that complex formation is the crucial factor that restricts the spin-label motion. The $\tau_r$ of the slow fraction is smaller than that of the protein complex, revealing that the spin label is not completely immobilized in the complex either due to local mobility or dynamics within the complex, such as motion of Cc relative to CcP in the encounter state.

No crystal structure of the Cc–SL bound to CcP is available, so Figure 7 shows a model of the spin label at the interface of the stereo-specific complex (ref. Figure 1c), using the structure of wild type Cc:CcP as obtained by X-ray crystallography.[32] The MTSL can just fit between the protein surfaces but inspection of possible conformations of the spin label, obtained by rotating it about the five torsion angles of the cysteine-SL adduct, shows that the motion must indeed be highly restricted, in agreement with the low mobility of the slow fraction observed by EPR.

To put these findings into perspective, we consider the properties of the complex from the EPR and the NMR results. Binding and dissociation of the Cc:CcP complex are fast on the NMR timescale, the lifetime being less than 1 ms. Information on the stereo-specific complex has been obtained from the crystallographic structure[32] and from previous NMR experiments,[40] however, such approaches are not able to

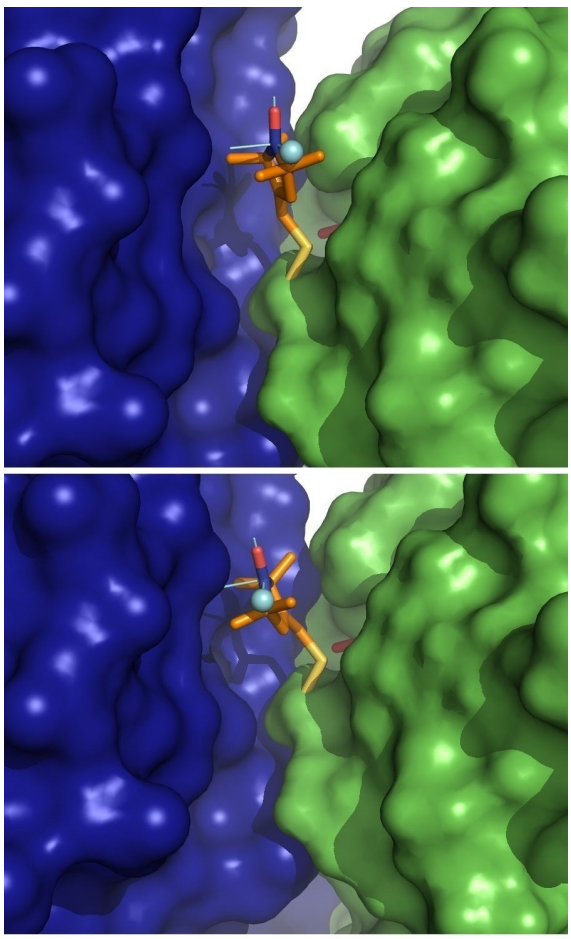

**Figure 7.** Two extreme orientations of the spin label in the interface of Cc and CcP: blue: CcP surface, green: Cc-surface with spin label attached. The cysteine is shown in yellow sticks, the spin label in orange, with the oxygen and nitrogen in red and blue, respectively. The axes of the g-tensor are shown in cyan lines with the $g_{yy}$ axis indicated with a small sphere. Haem of Cc: red sticks.

determine structural aspects of the encounter complex. The interconversion of stereo-specific and encounter complex of Cc–SL:CcP is expected to be (much) faster than the 1 ms timescale determined from the lifetime of the complex, but it is not clear whether it occurs on the ns or μs timescale.

From the fact that multiple components are detected in the EPR spectra, it can be concluded that the conversion between the states that give rise to these components are in slow exchange on the EPR timescale, i.e. slower than several ns (see SI). The two spectral components observed by EPR on the bound state of Cc show a ratio of 80% slow and 20% fast fraction, and are unlikely to represent spin-label mobility in the stereo-specific and the encounter complex, respectively: The encounter complex should be more dynamic than the stereo-specific one and according to NMR should contribute ~50%, i.e. much more than the 20% fast fraction observed in EPR. Figure 8, inset, illustrates a plausible distribution of the EPR components: The stereo-specific complex is entirely composed of the slow EPR fraction, so for the encounter complex 30% of the slow and 20% of the fast fraction remain. Thus, in the encounter state, 60% of the spin label has a mobility similar to that of the stereo-specific complex and 40% has a higher mobility. In Figure 8 possible spin-label arrangements are shown.

The EPR results enable us to build a bridge from the well-characterized stereo-specific complex to the elusive encounter complex: The majority fraction of the EPR response of the encounter complex (60%) is indistinguishable from the stereo-specific complex, suggesting a close similarity of the encounter with the stereo-specific complex in this respect. It certainly suggests a similar interface and that the Cc faces the CcP with the same protein face, restricting the spin label in the same way as in the stereo-specific complex. This interface may well resemble what is shown in Figure 7. In the remaining 40% of the encounter complex the higher mobility of the spin label suggests a looser interaction of the proteins, or a state in which the Cc surface containing the 81 residue is oriented differently with respect to the CcP (see Figure 8). Remarkably, the type of spin-label motion with preferred rotation about the $g_{yy}$ axis of the spin label in this fraction seems to be specific for the encounter complex. Our findings are in line with Brownian dynamics simulations on the encounter complex, based on electrostatic interactions, that showed that Cc interacts with CcP mostly with its 'front' side, the region around the haem edge, a finding that was supported also by NMR data.[33,63–65]

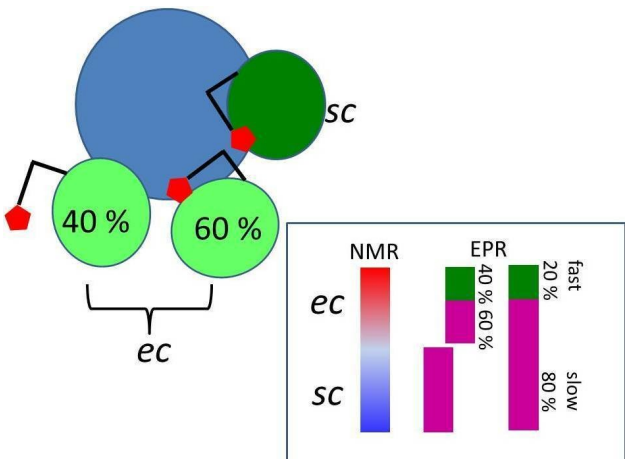


**Figure 8.** Schematic of complex properties. *ec*: encounter complex, *sc:* stereospecific complex. Inset: Complex components from NMR (left) and EPR (right) and their combination (center). Top: Cc in encounter complex (light green) with spin label (red pentagon) immobilized in the interface (60%) and free (40%). Cc in stereospecific complex (dark green).

We can also place some time constraints on the complex. Within the encounter complex, the Cc rotation cannot be faster than 1.2 ns or, if we consider the averaged rotation correlation time, 3 ns (see Table 1). Note that $\tau_r$ measures the spin-label mobility and therefore always gives the lower limit of the rotation correlation time of the protein to which the spin label is attached. In view of the correlation time of the spin label in free Cc (1.3 ns for the fast fraction, see Table 1) this is hardly surprising, given that it is not likely that the Cc rotates faster in the complex than on its own. More interesting is the finding that the interconversion between the stereo-specific-complex-like fraction and the more dynamic fraction is slow on the EPR timescale, suggesting a lifetime of the two fractions that is longer than 2–6 ns. A detailed description of the derivation of these time scales is given in the SI.

To summarize, we show an approach to analyse multi-frequency and in particular high-field, high-frequency EPR spectra of spin labelled protein-protein complexes, which enables us to obtain clean spectra of the bound state, a prerequisite to investigate the complex properties on the EPR time scale. In the present case, we choose a spin label position in the interface of the two proteins, enabling us to probe the local environment of the spin-label site. We show in particular that by high-field EPR a higher mobility component can be detected that would not have been seen by 9 GHz EPR and that the anisotropy of spin-label motion can be resolved, providing information on the space available at the site of the spin label. We suggest that the majority fraction of the encounter complex has interface properties similar to that of the stereo-specific complex. On the ns-timescale of EPR, this state is in slow exchange with a state that is less tightly bound than the previous one and in which the Cc may face the CcP differently than in the stereo-specific complex. In the future, we will extend this approach to other spin-label positions, to better map the properties of the encounter state, and also obtain further time constraints for the relative motion of the proteins in the encounter complex.

## Acknowledgement

*We thank Edgar Groenen for many fruitful discussions and the Dutch Science Organization (NWO) for funding (Grants 700.58.014 (MH) and 700.58.441 (MU))*

## Conflict of Interest

The authors declare no conflict of interest.

**Keywords:** cytochrome · high-field EPR · paramagnetic NMR · principal component analysis · transient protein complex

[1] A. N. Volkov, J. A. R. Worrall, E. Holtzmann, M. Ubbink, *Proc. Natl. Acad. Sci. USA* **2006**, *103*, 18945–18950.
[2] M. Ubbink, *FEBS Lett.* **2009**, *583*, 1060–1066.
[3] P. B. Crowley, M. Ubbink, *Acc. Chem. Res.* **2003**, *36*, 723–730.
[4] J. Schilder, M. Ubbink, *Curr. Opin. Struct. Biol.* **2013**, *23*, 911–918.
[5] Y. C. Kim, C. Tang, G. M. Clore, G. Hummer, *Proc. Natl. Acad. Sci. USA* **2008**, *105*, 12855–12860.
[6] K. Van de Water, N. A. J. van Nuland, A. N. Volkov, *Chem. Sci.* **2014**, *5*, 4227–4236.
[7] A. Spaar, C. Dammer, R. R. Gabdoulline, R. C. Wade, V. Helms, *Biophys. J.* **2006**, *90*, 1913–1924.
[8] S. Scanu, J. M. Foerster, G. M. Ullmann, M. Ubbink, *J. Am. Chem. Soc.* **2013**, *135*, 7681–7692.
[9] M. Harel, A. Spaar, G. Schreiber, *Biophys. J.* **2009**, *96*, 4237–4248.
[10] N. L. Fawzi, M. Doucleff, J. Y. Suh, G. M. Clore, *Proc. Natl. Acad. Sci. USA* **2010**, *107*, 1379–1384.
[11] W. Andralojc, Y. Hiruma, W. M. Liu, E. Ravera, M. Nojiri, G. Parigi, C. Luchinat, M. Ubbink, *Proc. Natl. Acad. Sci. USA* **2017**, *114*, E1840–E1847.
[12] M. Ubbink, M. Ejdeback, B. G. Karlsson, D. S. Bendall, *Structure* **1998**, *6*, 323–335.
[13] P. B. Crowley, G. otting, B. G. Schlarb-Ridley, G. W. Canters, M. Ubbink, *J. Am. Chem. Soc.* **2001**, *123*, 10444–10453.
[14] I. Diaz-Moreno, A. Diaz-Quintana, M. A. De la Rosa, P. B. Crowley, M. Ubbink, *Biochemistry* **2005**, *44*, 3176–3183.
[15] I. Diaz-Moreno, A. Diaz-Quintana, M. A. De la Rosa, M. Ubbink, *J. Biol. Chem.* **2005**, *280*, 18908–18915.
[16] J. A. R. Worrall, Y. J. Liu, P. B. Crowley, J. M. Nocek, B. M. Hoffman, M. Ubbink, *Biochemistry* **2002**, *41*, 11721–11730.
[17] J. A. R. Worrall, W. Reinle, R. Bernhardt, M. Ubbink, *Biochemistry* **2003**, *42*, 7068–7076.
[18] X. F. Xu, W. G. Reinle, F. Hannemann, P. V. Konarev, D. I. Svergun, R. Bernhardt, M. Ubbink, *J. Am. Chem. Soc.* **2008**, *130*, 6395–6403.
[19] M. Ubbink, D. S. Bendall, *Biochemistry* **1997**, *36*, 6326–6335.
[20] T. Selzer, G. Schreiber, *Proteins* **2001**, *45*, 190–198.
[21] F. B. Sheinerman, R. Norel, B. Honig, *Curr. Opin. Struct. Biol.* **2000**, *10*, 153–159.
[22] S. Scanu, J. M. Foerster, M. Timmer, G. M. Ullmann, M. Ubbink, *Biochemistry* **2013**, *52*, 6615–6626.
[23] G. M. Clore, J. Iwahara, *Chem. Rev.* **2009**, *109*, 4108–4139.
[24] G. Otting, in *Annual Review of Biophysics, Vol. 39* (Eds.: D. C. Rees, K. A. Dill, J. R. Williamson), Annu. Rev. Biophys., Palo Alto, **2010**, p. 387.
[25] V. P. Timofeev, V. V. Novikov, Y. V. Tkachev, T. G. Balandin, A. A. Makarov, S. M. Deyev, *J. Biomol. Struct. Dyn.* **2008**, *25*, 525–534.
[26] M. Sarewicz, A. Borek, F. Daldal, W. Froncisz, A. osyczka, *J. Biol. Chem.* **2008**, *283*, 24826–24836.
[27] M. Sarewicz, S. Szytula, M. Dutka, A. Osyczka, W. Froncisz, *Eur. Biophys. J. Biophys. Lett.* **2008**, *37*, 483–493.
[28] H. Jiang, A. M. English, *J. Inorg. Biochem.* **2006**, *100*, 1996–2008.
[29] D. Martins, M. Kathiresan, A. M. English, *Free Radical Biol. Med.* **2013**, *65*, 541–551.
[30] M. Kathiresan, D. Martins, A. M. English, *Proc. Natl. Acad. Sci. USA* **2014**, *111*, 17468–17473.
[31] Q. Bashir, A. N. Volkov, G. M. Ullmann, M. Ubbink, *J. Am. Chem. Soc.* **2010**, *132*, 241–247.
[32] H. Pelletier, J. Kraut, *Science* **1992**, *258*, 1748–1755.
[33] A. N. Volkov, Q. Bashir, J. A. Worrall, G. M. Ullmann, M. Ubbink, *J. Am. Chem. Soc.* **2010**, *132*, 11487–11495.
[34] M. A. Miller, *Biochemistry* **1996**, *35*, 15791–15799.
[35] M. A. Miller, L. Geren, G. W. Han, A. Saunders, J. Beasley, G. J. Pielak, B. Durham, F. Millett, J. Kraut, *Biochemistry* **1996**, *35*, 667–673.
[36] J. S. Zhou, B. M. Hoffman, *Science* **1994**, *265*, 1693–1696.
[37] E. D. A. Stemp, B. M. Hoffman, *Biochemistry* **1993**, *32*, 10848–10865.
[38] K. Van de Water, Y. G. J. Sterckx, A. N. Volkov, *Nat. Commun.* **2015**, *6*, 7073.
[39] A. N. Volkov, *Acc. Chem. Res.* **2015**, *48*, 3036–3043.
[40] J. A. R. Worrall, U. Kolczak, G. W. Canters, M. Ubbink, *Biochemistry* **2001**, *40*, 7069–7076.
[41] J. D. Satterlee, S. J. Moench, J. E. Erman, *BBA – Protein Struct M* **1987**, *912*, 87–97.
[42] O. Steinbock, B. Neumann, B. Cage, J. Saltiel, S. C. Muller, N. S. Dalal, *Anal. Chem.* **1997**, *69*, 3708–3713.
[43] J. Schilder, F. Lohr, H. Schwalbe, M. Ubbink, *FEBS Lett.* **2014**, *588*, 1873–1878.
[44] W. B. Pollock, F. I. Rosell, M. B. Twitchett, M. E. Dumont, A. G. Mauk, *Biochemistry* **1998**, *37*, 6124–6131.
[45] A. S. Morar, D. Kakouras, G. B. Young, J. Boyd, G. J. Pielak, *J. Biol. Inorg. Chem.* **1999**, *4*, 220–222.
[46] M. Guo, B. Bhaskar, H. Li, T. P. Barrows, T. L. Poulos, *Proc. Natl. Acad. Sci. USA* **2004**, *101*, 5940–5945.
[47] E. Lescop, P. Schanda, B. Brutscher, *J. Magn. Reson.* **2007**, *187*, 163–169.
[48] S. Grzesiek, A. Bax, G. M. Clore, A. M. Gronenborn, J. S. Hu, J. Kaufman, I. Palmer, S. J. Stahl, P. T. Wingfield, *Nat. Struct. Biol.* **1996**, *3*, 340–345.
[49] A. Kannt, S. Young, D. S. Bendall, *BBA –Bioenergetics* **1996**, *1277*, 115–126.
[50] S. Stoll, A. Schweiger, *J. Magn. Reson.* **2006**, *178*, 42–55.
[51] J. G. de la Torre, M. L. Huertas, B. Carrasco, *J. Magn. Reson.* **2000**, *147*, 138–146.
[52] A. N. Volkov, Q. Bashir, J. A. R. Worrall, M. Ubbink, *J. Mol. Biol.* **2009**, *385*, 1003–1013.
[53] A. N. Volkov, N. A. van Nuland, *J. Biomol. NMR* **2008**, *56*, 255–263.
[54] D. E. Budil, S. Lee, S. Saxena, J. H. Freed, *J. Magn. Reson. Ser. A* **1996**, *120*, 155–189.
[55] W. L. Hubbell, A. Gross, R. Langen, M. A. Lietzow, *Curr. Opin. Struct. Biol.* **1998**, *8*, 649–656.
[56] R. Langen, K. J. Oh, D. Cascio, W. L. Hubbell, *Biochemistry* **2000**, *39*, 8396–8405.
[57] M. A. Lietzow, W. L. Hubbell, *Biochemistry* **2004**, *43*, 3137–3151.
[58] H. J. Steinhoff, R. Mollaaghababa, C. Altenbach, H. G. Khorana, W. L. Hubbell, *Biophys. Chem.* **1995**, *56*, 89–94.
[59] M. G. Finiguerra, I. M. C. van Amsterdam, S. Alagaratnam, M. Ubbink, M. Huber, *Chem. Phys. Lett.* **2003**, *382*, 528–533.
[60] S. Scanu, J. Forster, M. G. Finiguerra, M. H. Shabestari, M. Huber, M. Ubbink, *ChemBioChem* **2012**, *13*, 1312–1318.
[61] J. Schilder, W. M. Liu, P. Kumar, M. Overhand, M. Huber, M. Ubbink, *Phys. Chem. Chem. Phys.* **2016**, *18*, 5729–5742.
[62] P. Fajer, M. Fajer, M. Zawrotny, W. Yang, in *Electron Paramagnetic Resonance Investigations of Biological Systems by Using Spin Labels, Spin Probes, and Intrinsic Metal Ions, Pt A, Vol. 563* (Eds.: P. Z. Qin, K. Warncke), **2015**, pp. 623–642.
[63] S. Lyubenova, M. K. Siddiqui, M. de Vries, B. Ludwig, T. F. Prisner, *J. Phys. Chem. B* **2007**, *111*, 3839–3846.
[64] R. R. Gabdoulline, R. C. Wade, *J. Mol. Biol.* **2001**, *306*, 1139–1155.
[65] S. Northrup, J. Boles, J. Reynolds, *Science* **1988**, *241*, 67–70.

Manuscript received: December 9, 2019
Revised manuscript received: February 3, 2020
Version of record online: April 17, 2020